Faraday Waves on a Viscoelastic Liquid

C. Wagner,[1] H. W. Müller,[2,3] and K. Knorr[1]
[1]*Institut für Technische Physik, Universität des Saarlandes, Postfach 151150, D-66041 Saarbrücken, Germany*
[2]*Institut für Theoretische Physik, Universität des Saarlandes, Postfach 151150, D-66041 Saarbrücken, Germany*
[3]*Max Planck Institut für Polymerforschung, Ackermannweg 10, D-55128 Mainz, Germany*
(Received 9 November 1998)

We investigate Faraday waves on a viscoelastic liquid. Onset measurements and a nonlinear phase diagram for the selected patterns are presented. By virtue of the elasticity of the material a surface resonance synchronous to the external drive preempts the usual subharmonic Faraday instability. Close to the bicriticality, the nonlinear wave interaction gives rise to a variety of novel surface states: sharply localized islands of hexagons or superlattices and hexagons or superlattices coexisting with line patterns of a different spatial periodicity length. Theoretical stability calculations on the basis of the rheometric viscosity data and qualitative resonance arguments support the experimental observations.

PACS numbers: 47.54.+r, 47.20.Ma, 47.50.+d

The generation of standing waves on the surface of a vertically vibrated Newtonian fluid (Faraday waves) is one of the classical hydrodynamic pattern forming instabilities [1]. Theoretical and experimental investigations during the last decade have substantially improved our understanding of the underlying processes [2]. Recently pattern formation in viscoelastic fluids has become the focus of nonlinear science, too. The memory of viscoelastic fluids introduces an additional time scale, which gives rise to a number of interesting phenomena [3–7]. It is amazing that Faraday [1] already tried to compare Newtonian fluids with viscoelastic ones: *"The difference between oil and white of egg is remarkable; . . . the crispated state may be a useful and even important indication of the internal constitution of different fluids."* Recently Raynal *et al.* [8] used a polymeric non-Newtonian fluid to investigate the wave dispersion and the threshold for the onset of Faraday waves. In Newtonian fluids the prevailing surface mode of the Faraday experiment is usually subharmonic (S) (i.e., the waves oscillate with twice the period of the external excitation). Nevertheless, for very thin layers the surface oscillation may become harmonic (H) (i.e., synchronous to the external drive [9–11]). However, the necessary vibration conditions are rather extreme, making this parameter region difficult to explore. On the other hand, for viscoelastic Maxwell fluids a theoretical analysis [12] predicts the harmonic Faraday resonance to preempt the usual subharmonic one, if the external drive frequency is comparable to the elastic relaxation time of the fluid. This prediction is based on the elasticity of the material and is independent of the filling level. Thus selecting a polymeric liquid with an appropriate elastic time scale will open a new way to a systematic investigation of the harmonic Faraday instability. We mention that a less direct but extensively used method of producing harmonic Faraday waves in Newtonian fluids is the two-frequency excitation introduced by Edwards and Fauve [13]. In the present paper, however, the drive signal is restricted to a single-frequency acceleration. It will be demonstrated that the harmonic resonance can be observed as a result of the elasticity of the fluid material. The interaction with the subharmonic mode gives rise to a variety of new pattern formation phenomena not yet observed in Newtonian fluids.

Our working fluid is a semidilute solution of 1.5 wt% PAA (polyacrylamide-co-acrylic acid, Aldrich 18,127-7, molecular weight 5×10^6 g/mol, average number of monomers 70 000). We use a 60:40 glycerol-water mixture (density $\rho = 1\,154$ kg/m^3) as a solvent to achieve a high static viscosity $\eta'(\omega = 0)$ far above 1 Pa s. For the polymeric solution the complex dynamic viscosity $\eta^\star(\omega) = \eta'(\omega) - i\eta''(\omega)$ has been measured at room temperature ($\simeq 22$ °C) with a cone plate viscometer (Rheometrics Fluids). Data acquisition was restricted to frequencies below $f = \omega/(2\pi) = 16$ Hz. However, within the range $1 < f < 16$ Hz the data could well be fitted by the following power laws: $\eta' = 0.244 \times \omega^{-0.594}$ Pa s and $\eta'' = 0.335 \times \omega^{-0.549}$ Pa s, where ω is measured in Hz. These relations have been used to extrapolate the viscosity data into the frequency range of our experiment ($30 < f < 100$ Hz). A rough estimate from the viscosity data yields an elastic relaxation time between 0.1 and 1 s. When approximating our polymeric solution with a Maxwell fluid we conclude that our experiment is operated in the overdamped regime of *free* surface waves [5]. Nevertheless, we do observe waves as they are *not free* but parametrically excited with an overcritical amplitude. The surface tension was determined independently by a ring tensiometer. We measured $\sigma = 0.067$ N/m, which deviates only slightly from the tabulated value for the water-glycerol solvent ($\sigma = 0.069$ N/m). The polymer PAA is a polyelectrolyte and therefore well soluble in a polar solvent. Demixing effects or concentration gradients close to the free surface or the container walls are not to be expected.

The experimental setup consists of a black container built out of anodized aluminum with an inner diameter of 290 mm, filled to a height of 3 mm with the working fluid. By means of an electromagnetic shaker the

 0031-9007/99/83(2)/308(4)$15.00

container is vibrated vertically with an acceleration $a\cos\Omega t$. The container is covered and sealed with a glass plate to prevent evaporation and pollution. Within a period of four weeks the experimentally observed scatter of the onset data did not exceed 1%. Because of the heat generation of the vibrator we were not able to work at room temperature, at which the rheometric viscosity data were taken. A heat wire filament regulates the temperature at $30 \pm 0.1\,^{\circ}\mathrm{C}$, measured by a positive temperature characteristic resistor imbedded in the bottom of the vessel. The vibration signal measured by a piezoelectric device (Bruel & Kjear 4393) proved to be sinusoidal with contributions from higher harmonics of not more than 2%. The surface patterns were recorded by a full frame CCD camera with an electronic shutter to allow for a discrimination between the H and S surface response. The phase diagram of the selected patterns is obtained by quasistatically ramping the drive amplitude from just below the onset $\epsilon = \frac{a}{a_c} - 1 = -5\%$ up to $\epsilon = 10\%$ (and vice versa) while keeping the frequency constant. During each scan the amplitude is increased by 1% steps and held constant for 300 s in between. Then, the surface of the fluid is photographed and the time dependence of the surface oscillation (whether S or H) is determined.

Figure 1 shows the threshold amplitude a_c and the critical wave numbers for the Faraday instability. By comparing with the corresponding curves for the pure Newtonian solvent the effect of viscoelasticity can easily be identified. The onset accelerations for both fluids closely compare at 70 Hz, while the increasing discrepancy towards lower frequencies indicates the typical frequency dependent shear thinning of viscoelastic liquids. Unlike Raynal *et al.* [8] we observe the dispersion relation (inset of Fig. 1) being largely affected by the elasticity. This might be a consequence of working at an elevated polymer concentration and with a more viscous solvent. Note that the surface tension σ is almost equal for both fluids. In the frequency domain above $f \simeq 60$ Hz the polymeric solution exhibits the usual subharmonic Faraday resonance with a surface pattern of lines. Since this behavior is similar to high viscosity "ordinary" liquids [13,14], we denote this region as the Newtonian regime. The present paper, however, is focused on the frequency range below 40 Hz, where the surface responds harmonically. The predominance of the harmonic Faraday resonance has recently been predicted for viscoelastic Maxwell fluids [12]. Note that the stability curve of the Newtonian solvent (dotted line in Fig. 1) gives no hint to a neighboring harmonic instability. By using the rheometric viscosity data for our polymeric solution we have computed the stability threshold (lines in Fig. 1) according to the method introduced by Kumar and Tuckerman [15]. To account for the viscoelasticity in [15] the linearized Navier-Stokes equation must be replaced by

$$\rho\,\partial_t v_\alpha = -\nabla_\alpha p + \rho g(t)\delta_{\alpha 3} + \nabla_\beta \sigma_{\alpha\beta}\,, \qquad (1)$$

where $\mathbf{v}(\mathbf{r},t)$ is the velocity field, $p(\mathbf{r},t)$ the pressure, and $g(t) = g_0 + a\cos\Omega t$ the modulated gravity acceleration. The Fourier transform $\sigma^*_{\alpha\beta}(\mathbf{r},\omega)$ of the viscoelastic stress tensor $\sigma_{\alpha\beta}(\mathbf{r},t)$ is given by $\sigma^*_{\alpha\beta}(\mathbf{r},\omega) = \eta^*(\omega)\dot\gamma^*_{\alpha\beta}(\mathbf{r},\omega)$, where $\dot\gamma^*_{\alpha\beta}$ is the Fourier transform of the velocity gradient tensor $\nabla_\alpha v_\beta$ and η^* the above defined complex viscosity. Reasonable agreement between theory and experiment is achieved except for frequencies close to the bicritical intersection point. Two possible causes of the discrepancy are the following: (i) There is a $7-9\,^{\circ}\mathrm{C}$ difference between the temperature of our experimental setup and that of the rheometer during the viscosity measurement. (ii) Errors due to the extrapolation of the viscometric data into the frequency range of our experiment.

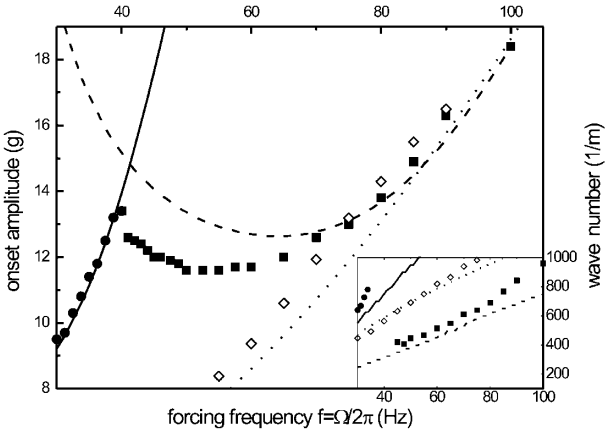

FIG. 1. The onset acceleration amplitude a_c and the critical wave numbers k_H and k_S. Solid circles (solid squares) denote the experimental data for the harmonic (subharmonic) branch of the polymeric mixture. Solid lines (dashed lines) represent the corresponding theoretical computation on the basis of the rheometric data $\eta^\star(\omega)$. Open diamonds and the dotted line are the respective results for the subharmonic branch of the Newtonian solvent. The associated harmonic branch is far beyond the parameter window shown.

Figure 2 depicts the phase diagram of the selected patterns. The surface structure in region IIa is a uniform pattern of hexagons covering the whole surface. In IIb we observe islands of hexagons (see Fig. 3a) surrounded by the flat surface state. The localization is extremely sharp and reflects the symmetry of the unit cells. A slight onset hysteresis up to 6% in ε is visible. The pattern selection processes for the backwards bifurcating hexagons in the harmonic region II and the forwards bifurcating lines in the subharmonic (Newtonian) regime V rely on the distinct respective time dependencies. This can be seen as follows (cf. also Ref. [13]): By taking the surface elevation η as a representative order parameter one has

$$\eta(\mathbf{r},t) = \left[\sum_m \begin{Bmatrix} H_m e^{i\mathbf{k}_{Hm}\cdot\mathbf{r}} \\ S_m e^{i\mathbf{k}_{Sm}\cdot\mathbf{r}} \end{Bmatrix} + \text{c.c.}\right] \times \sum_{n=-\infty}^{+\infty} \eta_n \begin{Bmatrix} e^{in\Omega t} \\ e^{i[n+(1/2)]\Omega t} \end{Bmatrix} \quad \text{for} \begin{Bmatrix} H \\ S \end{Bmatrix}. \qquad (2)$$

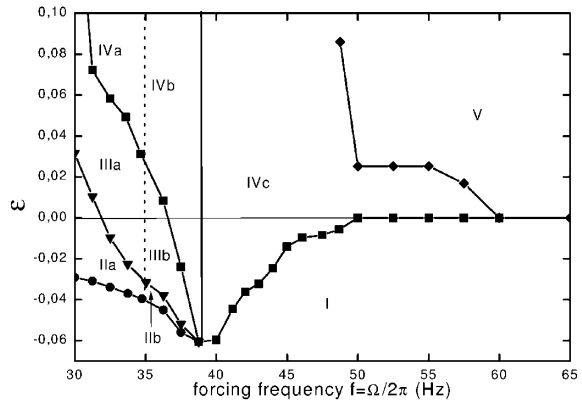

FIG. 2. Phase diagram of the observed nonlinear patterns. The symbols mark experimental data points. The abscissa, $\varepsilon = 0$, indicates the linear threshold shown in Fig. 1. The lowest solid line denotes the saddle point of the hysteresis. Region I: flat surface; IIa: harmonic hexagons covering the whole surface; IIIa: harmonic-subharmonic hexagonal superlattice (see text) extending over the whole surface; IIb, IIIb: as before but patterns occur in the form of localized patches surrounded by the flat surface; IVa, IVb, IVc: chaotic dynamics of subharmonic lines competing with extended (a) or localized (b) hexagonal superlattices or the flat surface (c); V: stationary subharmonic lines extending over the whole surface (Newtonian regime).

Here $\mathbf{r} = (x, y)$ is the horizontal coordinate, the lateral wave vectors $\mathbf{k}_{Hm}$ and $\mathbf{k}_{Sm}$, with $|\mathbf{k}_{Hm}| = k_H$ and $|\mathbf{k}_{Sm}| = k_S$ compose the spatial pattern, and the η_n are the temporal Fourier coefficients determined by the linear stability problem. Feeding η and a similar ansatz for $\mathbf{v}$ into an arbitrary quadratic nonlinearity results in a frequency spectrum of integral multiples of Ω, whether or not S or H are considered. Thus quadratic nonlinearities are able to resonate with *harmonic* linear eigenmodes, but not with *subharmonic* ones. Clearly, spatial resonance must be granted as well. Thus, any triplet of harmonic modes $\{\mathbf{k}_{H1}, \mathbf{k}_{H2}, \mathbf{k}_{H3}\}$ with $|\mathbf{k}_{Hm}| = k_H$ and $\mathbf{k}_{H1} + \mathbf{k}_{H2} + \mathbf{k}_{H3} = 0$ are in resonance. This generic 3-wave vector coupling is well known (e.g., from non-Boussinesq-Rayleigh-Bénard convection) and enforces a saddle node bifurcation towards hexagonal patterns.

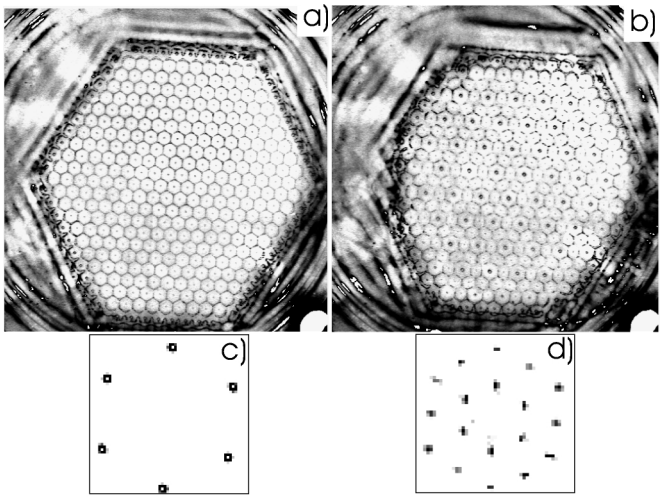

FIG. 3. Localized stationary surface patterns of harmonic hexagons (a) and the harmonic-subharmonic hexagonal superlattice (b) as observed in regions IIb and IIIb at $f = 37$ Hz and $\varepsilon = -0.05$ and -0.03. The corners of the picture show the outer edge of the container. In (c) and (d) the respective spatial Fourier spectra are shown. Patterns in regions IIa and IIIa are similar but they cover the whole surface.

Within the subharmonic region V such a resonant 3-wave vector coupling is prohibited due to the missing temporal resonance. Then the pattern selection mechanism is controlled by the cubic coupling coefficient in the associated amplitude equations [13,14,16]. Note that the subharmonic *temporal* symmetry $\eta(t + 2\pi/\Omega) = -\eta(t)$ for Faraday waves is analogous to the *spatial* up-down symmetry for Rayleigh-Bénard convection (known as the Boussinesq symmetry): They both prevent quadratic nonlinearities to appear in the amplitude equations.

If the drive amplitude is raised from II$a, b$ to IIIa, b, a sharp secondary transition can be detected: Subharmonic frequency contributions suddenly appear in the temporal Fourier spectrum of the surface elevation. Simultaneously the related spatial Fourier spectrum (Figs. 3c and 3d) exhibits a hexagonal superstructure with the same orientation, but with a wavelength twice as long as the primary one. These states are similar to the "type-II superlattice" seen by Kudrolli *et al.* [17] or the "SSS state" of Arbell *et al.* [18], who operated with a two-frequency excitation on Newtonian fluids. The underlying hexagonal substructures differ from ours by their relative size, orientation, and/or time dependence. Our theoretical stability calculations indicate that the *primary* subharmonic onset (dashed line in Fig. 1) is situated far above the nonlinear II-III transition. Therefore, the secondary superstructure must result from a nonlinear excitation process. The responsible mechanism is again a 3-wave vector interaction: Invoking basic resonance arguments, the subharmonic mode $\mathbf{k}_{S1} = \frac{1}{2}\mathbf{k}_{H1}$ with amplitude S_1 obeys the following amplitude equation (use cyclic permutation to get the equations for S_2 and S_3):

$$\partial_t S_1 = -\lambda S_1 + \chi H_1 S_1^{\star} + \text{higher order terms.} \quad (3)$$

Here $\lambda > 0$ reflects the linear damping and χ is a nonlinear coupling coefficient. According to Eq. (3) the secondary crossover from II to III occurs when the primary pattern amplitude $|H_m| = H$ exceeds the threshold $\lambda/|\chi|$. A comprehensive theoretical discussion of the selection process for superlattices can be found in Ref. [19].

The dashed line in Fig. 2 separating the subregions of homogeneous (a) and localized (b) hexagons is to be considered as an approximate boundary rather than a sharp transition line. By increasing f, the localized patches decrease in size until they disappear at $f > 39$ Hz. However, by keeping f fixed, their sizes do not

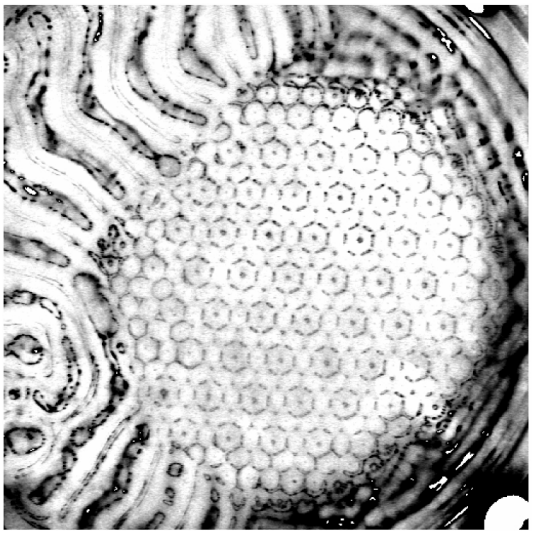

FIG. 4. Snapshot of a time dependent surface state in region IVb at $f = 37$ Hz and $\varepsilon = 2$. A stationary localized patch of hexagons is surrounded and competes with subharmonic lines moving in an erratic manner across the surface.

react to the forcing amplitude a. Note that the localized patches of hexagons cannot be explained by a triplet of real Landau equations supplemented by diffusive spatial derivatives: Within this familiar Ginsburg-Landau model, *stable* isolated islands of hexagons do not exist.

By entering region IVa or IVb the patterns become chaotically time dependent. Patches of subharmonically oscillating lines originating in an erratic manner from the cell boundary (a) or the flat surface (b) penetrate into the stationary hexagonal superlattice. Then they disappear again and the original structure is recovered. This process repeats itself on time scales of seconds to minutes, leading to a temporary coexistence of the stationary hexagonal superlattice with subharmonic lines (see Fig. 4). Higher driving amplitudes lead to a fully chaotic surface pattern.

For drive frequencies in the intermediate region IVc a similar chaotic behavior of subharmonic lines can be observed, however, as a result of a *primary* instability. Since hexagons do not occur beyond $f \simeq 39$ Hz, the subharmonic lines compete with the flat surface state. Nevertheless, the bifurcation still exhibits a small hysteresis, which continuously decreases as f approaches 60 Hz.

In conclusion, we have presented experimental results on Faraday waves in a viscoelastic medium. The predominance of the harmonic Faraday resonance predicted for ideal Maxwell fluids has been experimentally verified by means of a polymeric solution. The use of this liquid allows a systematic study of the pattern selection problem of synchronously responding Faraday waves without relying on the more complicated two-frequency excitation technique. The empiric onset data are found in quantitative agreement with the theory based on the rheometric viscometric data. Besides spatially homogeneous wave patterns of hexagons and superlattices we find very robust and sharply localized patches surrounded by the flat surface or—at higher driving amplitudes—in complicated dynamical competition with subharmonic lines. The spatially extended patterns are understood in terms of simple amplitude equations, while a theoretical understanding of the localized structures is still an ongoing problem.

We thank H. Rehage for the rheometry and for helpful comments. Furthermore, we acknowledge the support of J. Albers. This work is supported by the Deutsche Forschungsgemeinschaft.

[1] M. Faraday, Philos. Trans. R. Soc. London **52**, 319 (1831).
[2] For a review see J. W. Miles and D. Henderson, Annu. Rev. Fluid Mech. **22**, 143 (1990); H. W. Müller, R. Friedrich, and D. Papathanassiou, in *Theoretical and Experimental Studies of the Faraday Instability*, Lecture Notes in Physics, edited by F. Busse and S. C. Müller (Springer, New York, 1998).
[3] C. M. Vest and V. S. Arpaci, J. Fluid Mech. **36**, 613 (1969); M. Sokolov and R. I. Tanner, Phys. Fluids **15**, 534 (1972).
[4] H. R. Brand and B. J. A. Zielinska, Phys. Rev. Lett. **57**, 3167 (1986); B. J. A. Zielinska, D. Mukamel, and V. Steinberg, Phys. Rev. A **33**, 1454 (1986).
[5] H. Pleiner, J. L. Harden, and P. Pincus, Europhys. Lett. **7**, 383 (1988); J. L. Harden, H. Pleiner, and P. Pincus, J. Chem. Phys. **94**, 5208 (1991).
[6] R. G. Larson, E. S. Shaqfeh, and S. J. Muller, J. Fluid Mech. **218**, 537 (1990); R. G. Larson, Rheol. Acta **31**, 213 (1992).
[7] A. Groisman and V. Steinberg, Phys. Rev. Lett. **77**, 1480 (1996); **78**, 1460 (1997); Europhys. Lett. **43**, 165 (1998).
[8] F. Raynal, S. Kumar, and S. Fauve, Eur. Phys. J. B **9**, 175 (1999).
[9] K. Kumar, Proc. R. Soc. London A **452**, 1113 (1996).
[10] E. Cerda and E. Tirapegui, Phys. Rev. Lett. **78**, 859 (1997); J. Fluid Mech. **368**, 195 (1998).
[11] H. W. Müller, H. Wittmer, C. Wagner, J. Albers, and K. Knorr, Phys. Rev. Lett. **78**, 2357 (1997).
[12] H. W. Müller and W. Zimmermann, Europhys. Lett. **45**, 169 (1999).
[13] W. S. Edwards and S. Fauve, J. Fluid Mech. **278**, 123 (1994).
[14] P. Chen and J. Vinals, Phys. Rev. Lett. **79**, 2670 (1997).
[15] K. Kumar and L. S. Tuckerman, J. Fluid Mech. **279**, 49 (1994).
[16] H. W. Müller, Phys. Rev. Lett. **71**, 3287 (1993).
[17] A. Kudrolli, B. Pier, and J. P. Gollub, Physica (Amsterdam) **123D**, 99 (1998).
[18] H. Arbell and J. Fineberg, Phys. Rev. Lett. **81**, 4384 (1998).
[19] M. Silber and M. R. E. Proctor, Phys. Rev. Lett. **81**, 2450 (1998); M. Silber and A. C. Skeldon, Phys. Rev. E **59**, 5446 (1999).